Research Article

Permissive Conformations of a Transmembrane Helix Allow Intramembrane Proteolysis by γ-Secretase

Martin Ortner [1†], Nadja Guschtschin-Schmidt [2,3†], Walter Stelzer [1], Claudia Muhle-Goll [2,3] and Dieter Langosch [1*]

*1 - **Chair of Biopolymer Chemistry,** Technical University of Munich, Freising, Germany*
*2 - **Institute for Biological Interfaces 4,** Karlsruhe Institute of Technology, 76344 Eggenstein-Leopoldshafen, Germany*
*3 - **Institute of Organic Chemistry,** Karlsruhe Institute of Technology, 76131 Karlsruhe, Germany*

Correspondence to Dieter Langosch:*Lehrstuhl für Chemie der Biopolymere, Technische Universität München, Weihenstephaner Berg 3, 85354 Freising, Germany. *langosch@tum.de (D. Langosch)*
https://doi.org/10.1016/j.jmb.2023.168218
Edited by Yigong Shi

Abstract

The intramembrane protease γ-secretase activates important signaling molecules, such as Notch receptors. It is still unclear, however, how different elements within the primary structure of substrate transmembrane domains (TMDs) contribute to their cleavability. Using a newly developed yeast-based cleavage assay, we identified three crucial regions within the TMDs of the paralogs Notch1 and Notch3 by mutational and gain-of-function approaches. The AAAA or AGAV motifs within the N-terminal half of the TMDs were found to confer strong conformational flexibility to these TMD helices, as determined by mutagenesis coupled to deuterium/hydrogen exchange. Crucial amino acids within the C-terminal half may support substrate docking into the catalytic cleft of presenilin, the enzymatic subunit of γ-secretase. Further, residues close to the C-termini of the TMDs may stabilize a tripartite β-sheet in the substrate/enzyme complex. NMR structures reveal different extents of helix bending as well as an ability to adopt widely differing conformational substates, depending on the sequence of the N-terminal half. The difference in cleavability between Notch1 and Notch3 TMDs is jointly determined by the conformational repertoires of the TMD helices and the sequences of the C-terminal half, as suggested by mutagenesis and building molecular models. In sum, cleavability of a γ-secretase substrate is enabled by different functions of cooperating TMD regions, which deepens our mechanistic understanding of substrate/non-substrate discrimination in intramembrane proteolysis.

Introduction

The intramembrane aspartate protease γ-secretase is a promiscuous enzyme that is reported to cleave ∼150 substrates at positions that reside within the respective helical transmembrane domain (TMD).[1] Since these substrates represent only a small fraction of single-span membrane proteins, this prompts the question of how the protease distinguishes its substrates from non-substrates. In addition to a small extracellular domain being one requirement for cleavage by γ-secretase, its substrates share an N_{out} transmembrane topology. The mechanism of substrate/non-substrate discrimination may include initial substrate recognition by γ-secretase, the efficiency by which a cleavable site is translocated from the dry lipid bilayer towards the water-filled catalytic cleft, and the kinetics of bond scission. A pair of catalytic Asp residues is provided by TMDs 6 and 7 of

presenilin, the enzymatic component that forms the tetrameric γ-secretase complex together with nicastrin, presenilin enhancer 2 (PEN-2), and anterior pharynx defective protein (APH-1) at a 1:1:1:1 stoichiometry.[2,3] A shedded form of the amyloid precursor protein (APP), termed C99, is arguably the most intensely studied γ-secretase substrate. Shedding by β-secretase trims the extracellular domain of a substrate to a size not repelled by the gate-keeper subunit nicastrin,[4] which may also interact with a substrate.[5] Shedded APP is subject to multiple consecutive cleavages following initial endoproteolysis at ε-sites. This results in a mixture of A β peptides, longer forms of which are believed to cause Alzheimer's disease.[3,6] The recently determined cryo-electron microscopy (cryo-EM) structure of γ-secretase in complex with C83, another APP fragment, reveals helix unfolding around the initial cleavage sites as well as a small tripartite β-sheet consisting of residues downstream the initial cleavage sites and two domains of presenilin.[7] A similar picture holds for the γ-secretase complex with Notch1, another major substrate.[8] Initial Notch1 endoproteolysis at its S3 site close to the C-terminus of the TMD releases an intracellular fragment which translocates into the cell's nucleus where it activates a diverse set of genes involved in different cellular signaling pathways[9]; S3 cleavage is followed by cleavages at multiple S4 sites resulting in N β peptides.[10] The list of mammalian Notch paralogs includes Notch1, 2, 3, and 4.

γ-Secretase is a notoriously slow enzyme cleaving C99 and Notch1 on the scale of minutes.[4,11] Since model helices in aqueous solution tend to unfold within nanoseconds[12] the rate of TM helix unfolding is unlikely to limit the rate of proteolysis and is therefore implausible to contribute to substrate selection. This is consistent with mutational studies having failed to provide a clear link between helix flexibility near the scissile endoproteolytic sites of C99 and its cleavability.[13–18] An intriguing structural feature of the APP TMD is a hinge at a VGGV motif within its N-terminal half (TM-N) as shown by NMR spectroscopy[19,20] and molecular dynamics simulations.[21,22] It has been proposed that one mechanism by which γ-secretase accepts a substrate TMD may depend on a conformationally flexible TM-N enabling the scissile bond to translocate from the periphery of presenilin towards its catalytic cleft (reviewed in [23–25]). Indeed, mutations altering the conformational flexibility at the VGGV hinge affect the efficiency and specificity of C99 cleavage.[22,26] Apart from the APP TMD, first evidence for the existence of a flexible TM-N has previously been obtained for the Notch1 TMD. Although the Notch1 TMD essentially forms a canonical α-helix in mixed detergent/lipid bicelles,[27,28] deuterium-hydrogen exchange (DHX) studies in a more polar solvent revealed increased helix flexibility near an AAAA motif within its TM-N.[18,29] At this motif and at some other sites, the helix appears indeed distorted within the γ-secretase/Notch1 complex.[8] The AAAA motif contains multiple S4 cleavage sites[30] and mutating individual Ala residues had previously altered the specificity and efficiency of S4 cleavage.[31]

Here, we characterized the Notch1 and Notch3 TMDs in terms of cleavability in a newly established assay system, conformational flexibility, and 3D-structure. We report that the different cleavabilities of both paralogs correspond to different extents of TMD helix curvature. Mutations at the AAAA motif altering the cleavability of the Notch1 TMD scale with conformational flexibility. By contrast, mutations covering the initial cleavage site confirm the dependence of cleavability on local sequence but not on local helix flexibility. The impact of mutations downstream the initial cleavage site suggests that formation of the tripartite β-sheet may support substrate/non-substrate discrimination.

Results

Our approach was to combine cleavage efficiency of wt and mutant substrates with the conformational flexibility of selected TMD helices obtained by DHX as well as with 3D-structures determined by NMR spectroscopy (Figure 1).

A novel yeast-based assay to assess γ-secretase activity

Initially, we developed a novel yeast-based assay system to monitor γ-secretase-mediated cleavage in a biological membrane. In this yeast based tool, the γ-secretase subunits presenilin 1, nicastrin, APH-1a, and PEN-2 are expressed from genomically integrated reading frames. Chimeric constructs encoding a signal sequence, substrate, green fluorescent protein (GFP) for quantification and visualization, and the transcription factor GAL4 are plasmid-borne to ensure that the concentration of a substrate exceeds that of the γ-secretase complex. Cleavage of a membrane-bound substrate releases soluble GAL4p that transfers to the nucleus to activate the *lacZ* gene, thus driving expression of β-galactosidase (β Gal). β Gal activity reports the efficiency of endoproteolysis (Figure S1(a)). To validate the system, we first compared the β Gal activities of C-terminal fragments of the different Notch receptor paralogs and APP. All substrates were designed to be of equal length (100 residues) for optimal comparability (C100 = C99 plus an N-terminal Met[32]). A rank order of cleavability of Notch1 > C100 > Notch3 (Figure 2) is in line with previous comparisons in eukaryotic[16,33] and yeast[34] cells. That Notch cleavage depends on the sequence of its TMD is shown by the resistance of Notch1-L24 to cleavage, this construct contains a

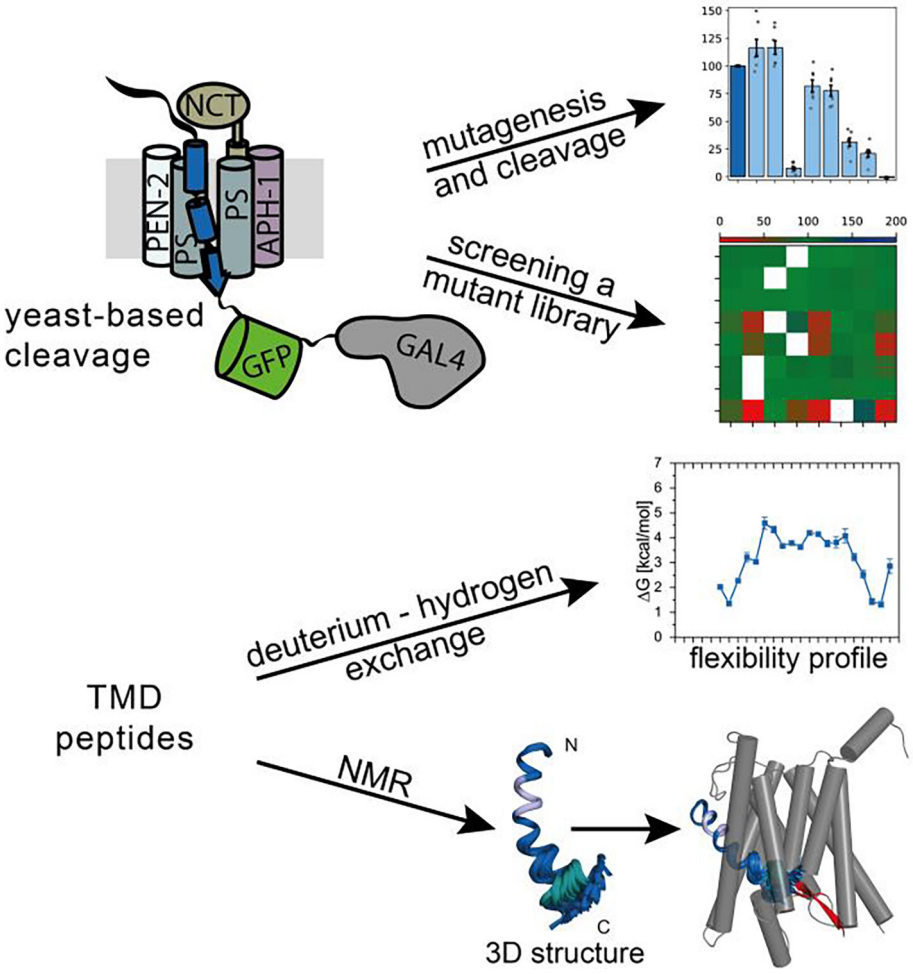

Figure 1. Outline of experimental approaches combined in this study.

24-residue oligo-Leu sequence in place of its natural TMD. A conformationally rigid oligo-Leu TMD was previously shown to render C100 a non-substrate.[18]

In control experiments, we routinely compared β Gal expression in cells with or without γ-secretase. The results clearly show that the cleavage of Notch1, Notch3, and C100 depends on γ-secretase. We note, however, that Notch2 cleavage did not depend on γ-secretase and that Notch4 was not cleaved (Figure S1(b), upper panel). Measuring GFP fluorescence of cells confirmed similar levels of the chimeric proteins (Figure S1(b), lower panel). The dependence of Notch1, Notch3, and C100 cleavage on γ-secretase was also shown by the inability of the presenilin 1 D385A mutant to support their cleavage (Figure S1(c)). Mutation of the catalytic D385 renders presenilin inactive.[35] Further, incubation of the cells with the well-established γ-secretase inhibitor LY-411,575[36] resulted in dose-dependent reductions of C100, Notch1, and Notch3 cleavage (Figure S1(d)); this provides further proof of the dependence of cleavage on γ-secretase. The subcellular localization of our exemplary substrates was assessed by confocal microscopy visualizing the GFP moiety. To our surprise, C100, Notch1, and Notch3 were identified in the vacuolar membrane, rather than in the plasma membrane (Figure S1(e)) thus suggesting the vacuole to be the site of γ-secretase-mediated substrate cleavage. Vacuolar localization was also seen for the Notch1-L24 protein, thus demonstrating that even exchanging the complete wt TMD to an artificial sequence does not affect sorting.

Taken together, our assay faithfully reproduces the cleavage and its pharmacological inhibition of Notch1, Notch3, and C100, consistent with data obtained from other assay systems.[16,33,37] The underlying cleavage events presumably occur at the S3 site or ε-sites, respectively. To our knowledge, we report for the first time that substrates preferentially localize to the vacuole of the yeast cell.

Identifying TMD regions that define Notch cleavage by γ-secretase

Here, we mapped the domains of Notch TMDs that determine their cleavability using Notch1 and

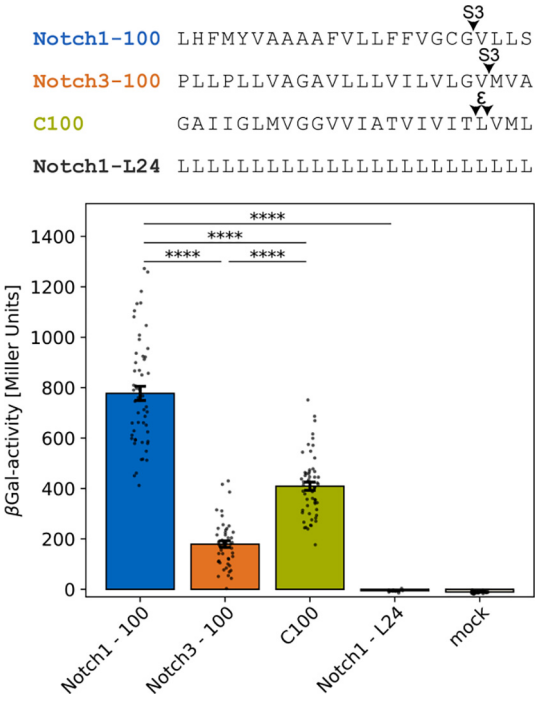

Figure 2. Validation of the yeast-based assay system. The bars represent β Gal activities in Miller Units. Data are represented as means ± SEM (n = 13–54 biological replicates). Statistical significance was assessed using one-way ANOVA paired with Tukey's multiple comparison test (*: p < 0.05, **: < 0.01, ***: p < 0.001, ****: p < 0.0001). Controls documenting residual γ-secretase-independent cleavage and substrate expression levels are given in Figure S1.

Notch3, the paralogs being clearly subject to γ-secretase cleavage in yeast. First, we tested the impact of replacing the Notch1 or Notch3 TM-Ns or TM-Cs by those of the respective paralog. The Notch3 TM-C decreased cleavability of the corresponding Notch1-100 derivative almost to the level of wt Notch3-100, while the Notch3 TM-N had no detectable effect (Figure 3(a,b)). Likewisely, the Notch1-TM-C slightly, yet significantly, increased cleavage of the Notch3-100 derivative, while the Notch1 TM-N was again ineffective. Hence, TM-C at least partially defines the difference in Notch1 *vs* Notch3 cleavage, while TM-N does not.

To explore the TMDs at more detail, we tested the effects of replacing overlapping sets of four consecutive wt TMD residues by Leu tetrads (Figure 3(c,d)). Within the Notch1 TMD, one of the most sensitive regions corresponds to the AAAA motif within its TM-N. This motif had previously been suggested to form a flexible site within the TM helix, similar to the cleavage-promoting VGGV hinge of APP C100.[29] Indeed, the AAAA to LLLL substitution in Notch1-100 (Figure 3(d)) was as effective as the VGGV-to-LLLL substitution in C100 (see Figure 4), reducing cleavage by >90%.

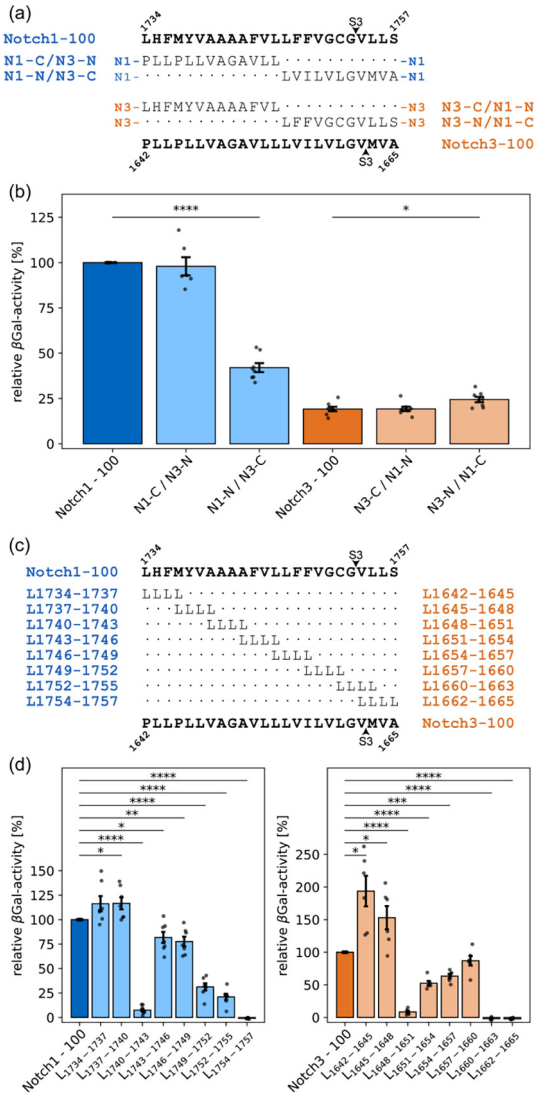

Figure 3. Detailed mapping of regions being important for γ-secretase-mediated cleavage. (a) Sequences used to assess the consequences of swapping TM-N *vs* TM-C in corresponding chimeric constructs. **(b)** β Gal activities normalized to wt Notch1-100 (=100%). Shown are means ± SEM, n = 6–8. For statistical comparisons of data containing Notch1-100, one-sample t-tests were used, comparisons between all other samples utilized two-tailed t-tests. **(c)** Sequences generated by Leu tetrad scanning mutagenesis. **(d)** β Gal activities normalized to wt Notch1-100 (left panel) or wt Notch3-100 (right panel (=100%). Shown are means ± SEM, n = 6–7. Statistical significance was assessed using one-sample t-tests with the corresponding wt = 100% as reference (*: p < 0.05, **:p < 0.01, ***: p < 0.001, ****: p < 0.0001). Controls documenting residual γ-secretase-independent cleavage as well as substrate expression levels are given in Figure S2.

Another sensitive region extends from Notch1 F1749 to S1757 within TM-C. This region harbors the S3 cleavage site between G1753 and V1754.

Further, the sequence L1755-L1756-S1757 at the very C-terminus forms a tripartite ß-sheet with residues at the N-terminus of presenilin TMD 7 and the loop connecting TMD 6 and TMD 7 in the structure of the Notch1/γ-secretase complex. The sheet is believed to stabilize the unfolded state of the region around the S3 site, thus preparing it for cleavage.[38] Interestingly, mutating this sheet-forming region had a stronger impact on cleavage than mutating the residues around S3. A similar picture emerged for Notch3. Replacing an AGAV motif within its TM-N by LLLL again abolished cleavage (Figure 3 (c,d)). Within TM-C, the region from L1660 to V1663, holding the S3 site, as well as the presumably sheet-forming sequence from V1662 to A1665 proved to be most sensitive. In addition, a region near the N-terminus of the Notch3 TMD appears to be important as the cleavabilities of Notch3-$L_{1642-1645}$ and $L_{1645-1648}$ exceeded that of the wt by ∼100% and ∼50%, respectively. The mutated residues include one or both Pro residues within TM-N. Pro at a helix N-terminus is known as N-capping residue with a helix-stabilizing function[39] while Pro within a helix is destabilizing.[40]

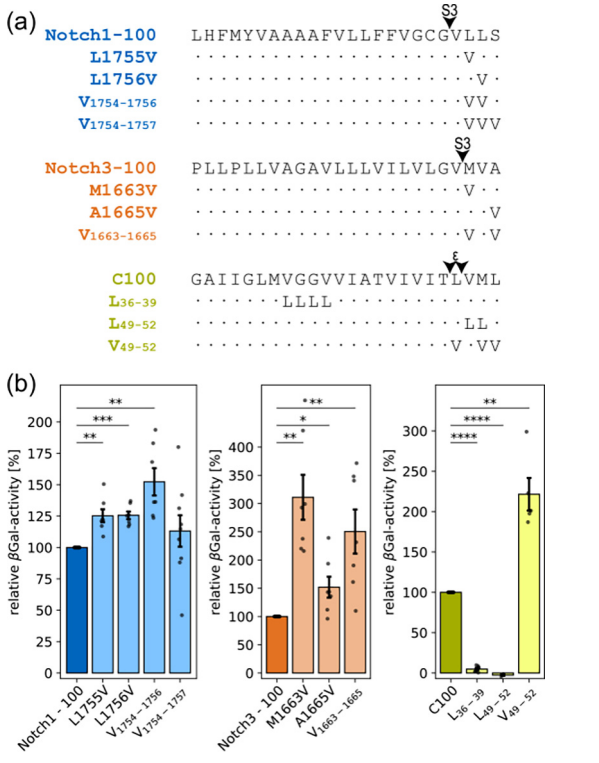

Figure 4. Investigating the β-sheet-forming TMD region for its role in cleavage. (a) Sequences analyzed for cleavage. **(b)** β Gal activities normalized to the corresponding wt sequence (left panel: Notch1-100; center panel: Notch3-100; right panel: APP C100). Shown are means ± SEM, n = 7–9. Statistical significance was assessed using one-sample t-tests with the corresponding wt set to 100% as control condition (*: $p < 0.05$, **:$p < 0.01$, ***: $p < 0.001$, ****: $p < 0.0001$). Controls documenting residual γ-secretase-independent cleavage as well as substrate expression levels are given in Figure S3.

Next, we replaced residues within the sheet-forming Notch1 L1755-L1756-S1757 sequence by Val, hypothesizing that this β-branched amino acid, which is known to favor β-sheet formation,[41] might enhance cleavage through stabilizing the tripartite β-sheet with presenilin. Indeed, single Val mutations enhanced cleavability by ∼25% and the effects added up in the double mutant that contains a VVV motif together with the natural V1754 (Figure 4). However, a triple mutant resulting in a VVVV motif behaves similar to the wt indicating a functional role of S1757 at the very TMD C-terminus. In case of Notch3, creating a VVV motif by the M1663V mutation tripled cleavage while extending this to a VVVV motif had a lesser impact again pointing to a role of the very C-terminal A1665. To test whether the impact of Val can be reproduced with the APP C100 TMD, we replaced four residues near its C-terminus by a VVVV motif which increased cleavage >2-fold. By contrast, replacing M50 and V51 by Leu, that has a low propensity to form β-sheets,[41] abolished cleavage.

The Notch1 TM-C from V1750 to S1757 was mapped for sensitive residues at a more granular level by mutations to hydrophobic amino acids, including Pro. For efficiently determining cleavage of the resulting 64 point mutants, we created a library of mutants that was subjected to a selective screen using a yeast strain containing an auxotrophic marker under control of a GAL4 responsive element. This approach was validated by confirming that the read-out of the screen, i.e., the abundance of sequences under selective conditions, correlates very well (R^2 = 0.96) with the β Gal activities of selected constructs (Figure S4). The most sensitive amino acids correspond to the S3 site residues G1753 and V1754 as well as S1757 (Figure 5).

The mutational data were complemented by the design of Notch-based minimal substrate TMDs. Having shown that the poly-Leu TMD in Notch1-L24 resists cleavage (Figure 2), we used poly-Leu as a template in a gain-of-function approach. Minimal cleavable TMD sequences were stepwisely reconstructed from cleavage-supporting regions identified above. Finding that a GGGG motif within TM-N (Notch1-$G_{1740-1743}$) supports Notch1-100 cleavage even better than the natural AAAA sequence (Figure 6), we initially employed GGGG in our gain-of-function approach. In short, we find that the GGGG motif cooperates well with a VVVS motif downstream of S3 (construct TMD4), but not with the GCG motif preceding the S3 site (TMD2). The most efficiently cleaved minimal TMD comprises GGGG, GCG, and VVVS (TMD5); this sequence is processed with an efficiency well above that of wt

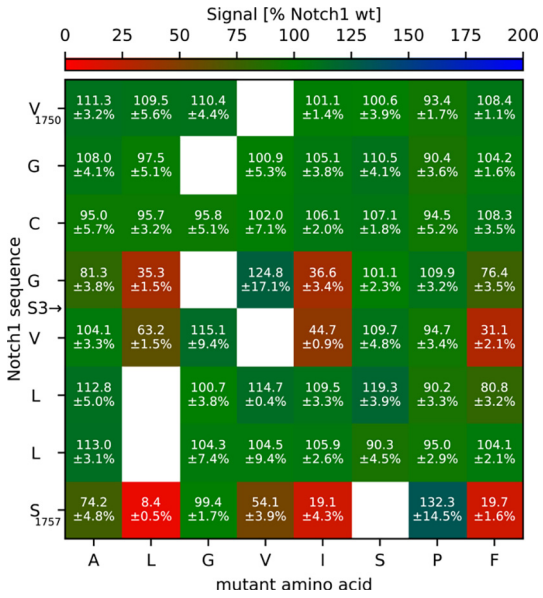

Figure 5. Detailed mutational screen of the Notch1 TM-C using a library selection approach. The mean signals (±SEM, *n* = 4 independent screens) were derived from the abundance of sequences, as determined by deep sequencing, under selective conditions and normalized to wt Notch1-100 (=100%). Color coding reflects the exents of cleavage.

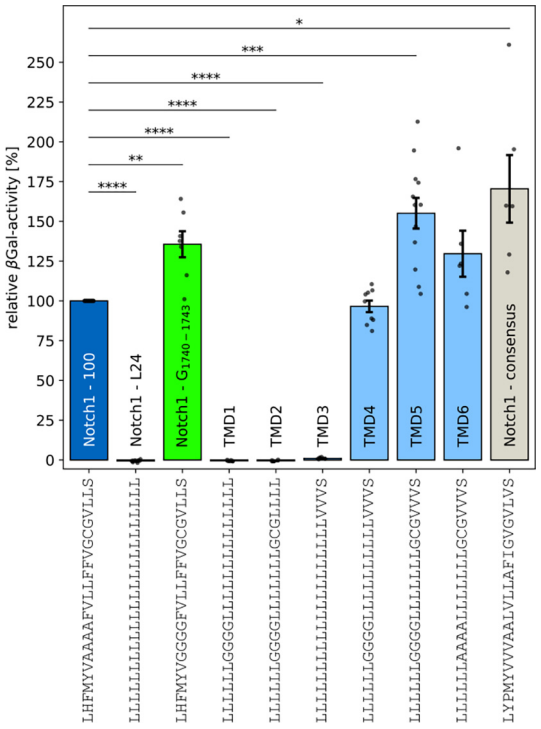

Figure 6. Designing artificial substrate TMDs. Using Notch1-L24 as template, mimimal substrate TMDs 1 to 6 were generated by grafting key sensitive regions onto the poly-Leu TMD. The Notch1-consensus was identified by analyzing pairwise sequence alignments of Notch1 TMD orthologs after BLAST (Figure S6). Data were normalized to the corresponding wt Notch1-100 sequence (=100%) and are presented as means ± SEM (*n* = 6–13). Statistical significance was assessed using one-sample t-tests with Notch1-100 wt as control condition. (*: $p < 0.05$, **: $p < 0.01$, ***: $p < 0.001$, ****: $p < 0.0001$). Controls documenting residual γ-secretase-independent cleavage as well as substrate expression levels are given in Figure S5.

Notch1-100. The natural AAAA motif is less supportive than GGGG (compare TMD5 to TMD6) (Figure 6).

Finally, we examined the extent of amino acid conservation of our substrate TMDs across a wide range of species by BLAST analysis within vertebrate orthologs. While the APP TMD is almost completely conserved (Figure S6), Notch TMDs display significant sequence variability (Figure S6). The consensus motifs in place of Notch1 AAAA and Notch3 AGAV correspond to VVAA and GAAA, respectively. Among the most highly conserved residues rank Notch1 G1753 / Notch3 G1661 near the S3 sites as well as Notch1 S1757 / Notch3 A1665 at the very C-termini of the TMDs. In addition, several other positions are well conserved. Since these other positions were not required for reconstructing our well-cleaved TMD6 model (Figure 6), they may support Notch functions other than cleavability by γ-secretase. Cleavage of the Notch1 consensus TMD was ~65% above that of wt Notch1-100. To assess to which extent the cleavage-promoting effect of a GG motif depends on its precised location within TM-N, we tested a range of constructs based on minimal TMD5 with GG at different positions. These TMDs are well cleaved, except construct GG+2 where GG located at the TM-N/TM-C junction was less supportive than at positions closer to the AA sequence of the VVAA consensus (Figure S7).

Control experiments verified that cleavage of all substrate constructs was negligible in cells not expressing γ-secretase, thus ruling out that increased cleavability could result from their exposure to other proteases. Also, the expression levels of wt and mutants were roughly similar, thus excluding differing levels of protein expression as a source of differential β Gal production (Figures S2–S5, S7).

Taken together, our results identify three most crucial regions within the Notch TMD that cooperate in forming a well cleavable sequence. While the AAAA/AGAV motifs within the TM-N are likely to confer conformational flexibility, the crucial regions within TM-C may support sheet formation with presenilin and docking of the S3 cleavage region into the catalytic cleft of presenilin. The difference between Notch1 and Notch3 is partially defined by TM-C, but not by TM-N.

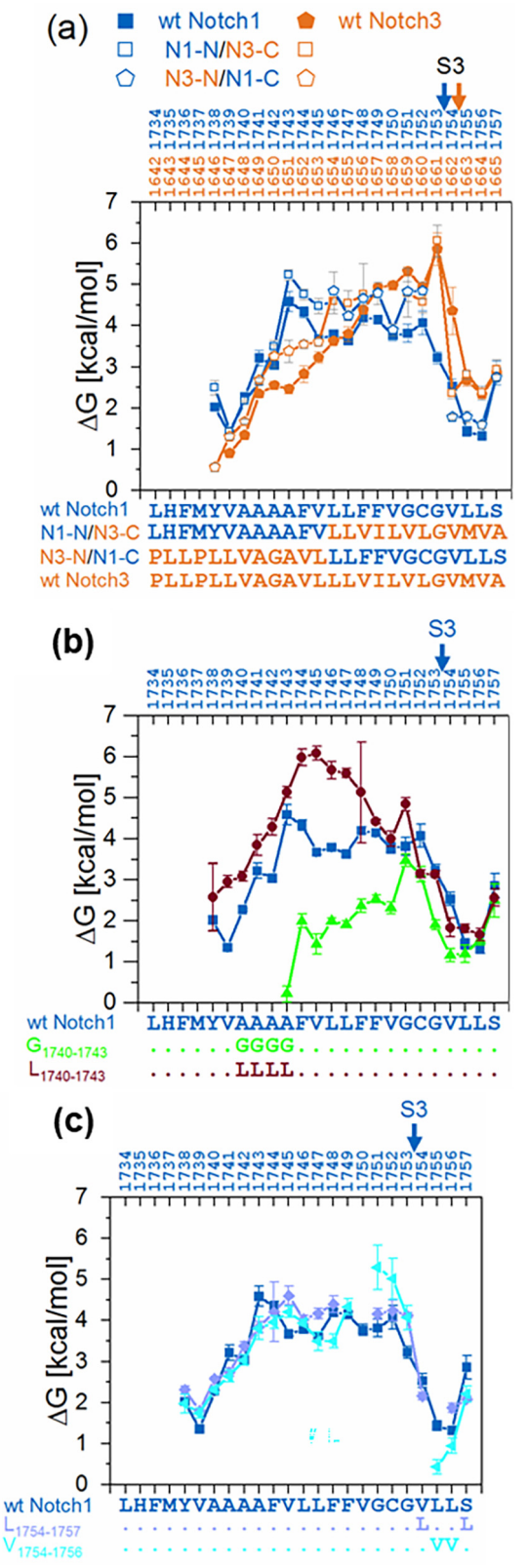

Deuterium/hydrogen exchange uncovers the impact of sequence on conformational flexibility

In order to examine the dependence of Notch cleavability on TM helix flexibility, we performed DHX analysis of TMD peptides. Similar to previous analyses,[18,21,22,29,42] DHX kinetics of exhaustively (>95%) deuterated synthetic peptides (Table S1) were analyzed in 80% trifluoroethanol (TFE). The polarity of TFE roughly matches that within the solvated interior of a protein[43]; TFE is therefore thought to mimic the aqueous environment at the presenilin catalytic cleft.[44]

Overall amide hydrogen exchange kinetics of Notch1 TMD peptides reveal that TM-N mutations have a stronger impact on helix flexibility than TM-C mutations (Figure S8). As expected, the DHX kinetics of the wt is clearly different from those of the slower $L_{1740\text{-}1744}$ mutant and the faster $G_{1740\text{-}1744}$. By contrast, mutants $V_{1754\text{-}1756}$ and $L_{1754\text{-}1757}$ were similar to the wt TMD. Residue-specific DHX kinetics where obtained after gas-phase fragmentation of peptides at different time points (Figure S9). From the corresponding exchange rate constants k_{exp} (Figure S10) we calculated the respective free energy changes ΔG of amide H-bond opening. Their distributions along the TMD sequences are referred to as 'flexibility profiles' (Figure 7).

A comparison of wt Notch1 and wt Notch3 TMDs reveals that the Notch3 TM-N tends to exhibit lower amide H-bond strengths than its Notch1 counterpart, specifically at Notch3 positions A1651 and V1652 directly downstream of G1650. By contrast, the TM-C of Notch3 is more stable than the Notch1 TM-C, which may result from the presence of two Gly residues within Notch1 *vs* only one Gly within Notch3 (Figure 7(a)). Analyzing the Notch1/Notch3 hybrid TMDs showed that the flexibility profiles of TM-N and TM-C are roughly similar to those in the respective wt TMDs (Figure 7(a)) although we note some mutual influence of TM-N on TM-C and *vice versa*, possibly mediated via side-chain/side-chain interactions across the TM-N/TM-C boundaries. The flexibility profiles of the mutant Notch1 TMDs

Figure 7. Residue-specific helix flexibility as determined by DHX. (a) Comparison of wt Notch1, wt Notch3 (filled symbols), and chimeric TMDs. (b) Wt Notch1 and its $L_{1740\text{-}1744}$ or $G_{1740\text{-}1744}$ mutants. (c) Wt Notch1 and its $L_{1754\text{-}1757}$ or $V_{1754\text{-}1756}$ mutants. Amide H-bond stabilities ΔG were calculated from k_{exp} and $k_{exp,b}$ values given in Figure S10. Sequence positions are given above the graphics. Wt Notch1 data are reproduced.[18] Error bars correspond to standard confidence intervals (calculated from the errors of fit in k_{exp} determination, in some cases smaller than the symbols, n = 3 independent DHX reactions).

revealed that replacing the Notch1 AAAA motif by Leu in mutant $L_{1740\text{-}1743}$ stabilizes the complete TM-N while its replacement by Gly in mutant $G_{1740\text{-}1743}$ led to strong and broad destabilization. In both cases, H-bond stabilities are altered by up to ~2 kcal/mol (Figure 7(b)). These effects are in agreement with the known impacts of these amino acid types on helix stability.[45–47] By contrast, the impacts of introducing two Leu or Val residues at the very C-terminal tetrad of residues (mutants Notch1 $L_{1754\text{-}1757}$ and $V_{1754\text{-}1756}$), where the wt helix is only marginally stable, are much more nuanced. $V_{1754\text{-}1756}$ appears to be stabilized at position 1751 and destabilized at position 1755 by ~1 kcal/mol, relative to wt Notch1 (Figure 7(c)).

In sum, the TMDs of Notch1 and Notch3 differ markedly in their flexibility profiles. Mutating the Notch1 AAAA to Leu or Gly results in pronounced TM helix stabilization or destabilization, respectively. By contrast, mutations near the unstable C-terminal helix had only marginal effects.

NMR spectroscopy unravels the structure of Notch TMDs

The 3D structures of wt Notch1 and wt Notch3 TMDs, as well as of Notch1 $L_{1740\text{-}1743}$ and Notch1 $G_{1740\text{-}1743}$ were determined by NMR spectroscopy. We intended to unravel how primary structure affects helicity and how this may affect the interaction of the TMDs with presenilin. To this end, we determined secondary chemical shifts $\Delta\delta$, defined as the difference between random coil and observed values, as well as characteristic nuclear Overhauser effect (NOE) contacts. Negative $^{1}H_{\alpha}$ and $^{13}C_{\beta}$ $\Delta\delta$, as well as positive $^{13}C_{\alpha}$ $\Delta\delta$ values are characteristic of a helical conformation.[48] In ^{1}H 2D NOESY spectra, a continuous series of short-range NOE crosspeaks (dNN(i, i+2), dαN(i, i+3), d$\alpha\beta$(i, i+3)) independently identifies a helix.[49] Additional dαN(i, i+4) NOEs are present in α-helices, while dαN(i, i+2) crosspeaks only occur in 3_{10} helices.[50,51] Our data show that the wt Notch1 peptide is α-helical from L1734-S1757. The Notch3 helix is shorter based on the chemical shifts (L1646-A1665, presumably resulting from the presence of Pro residues near its N-terminus (Figures S10(a) and S11). Helicity is relatively low within the TM-N of both paralogs, as demonstrated by the absence of dNN(i, i+2) NOEs and occurrence of dαN(i, i+2) NOEs for the wt as well as by reduced $^{13}C_{\alpha}$ and $^{1}H_{\alpha}$ $\Delta\delta$, especially around the Notch1 AAAA and the Notch3 AGAV motifs. Likewise, simultaneous dαN(i, i+2) and dαN(i, i+4) NOEs suggest a disruption of the regular α-helix directly upstream of the S3 cleavage sites (Figure S11). Calculating the chemical-shift-derived helicity and order parameter S^2 with TALOS+[52] confirms a slightly less rigid and less helical conformation at these sites (Figure S12).

The overall structure of the wt Notch1 TMD exhibits a bend (Figures S10(a) and S13). When the 40 structural models of lowest energy were superimposed from L1734 to L1747 at their TM-N, the TM-C helices fanned out thus forming a defined cone. Viewing the bundle from the N-terminus, the concave side of the helix is lined by residues A1742, V1745, F1749, and C1752 while the bulky amino acids F1744, L1747, F1748, and V1750 are located on the convex side (Figure S14). In case of the mutant Notch1 $L_{1740\text{-}1743}$, secondary chemical shifts and characteristic NOE contacts (Figure S11) indicate a general stabilization of the helix, which is most pronounced at the mutated site. Presumably due to the larger Leu side chains, the helix is more straight than that of wt Notch1 (Figures S10(c) and S13). Further, the fanning out of TM-C in the bundle is less pronounced and the mean direction of TM-C in the bundle is turned by ~60°. By contrast to that, replacing the AAAA motif by Gly in Notch1 $G_{1740\text{-}1743}$ resulted in a collapse of secondary structure at this site. This is demonstrated by the loss of characteristic NOEs, reduced $^{13}C_{\alpha}$ and $^{1}H_{\alpha}$ $\Delta\delta$ (Figure S11), as well as a significantly lower order parameter S^2 (Figure S12). The TM-Cs of both mutants are of comparable helicity and order to wt Notch1. Due to the small Gly side chain, significantly less NOE contacts could be identified near them, so that this part is structurally ill-defined. Therefore, the orientation of TM-N relative to TM-C is less constrained by the data. Consequently, the structural bundle of the Notch1 $G_{1740\text{-}1743}$ TMD has an extraordinarily wide distribution of possible TM-N *vs* TM-C orientations. However, this distribution is not completely arbitrary in showing a preferred TM-C direction (Figures S10(c) and S13). The TMD helix of wt Notch3 is rather straight (Figures S10(b) and S13). A slight bending was deflected towards residues L1646, G1650, L1653, and G1661, which are located at the concave side while residues V1648, V1652, L1655, and V1659 form the convex side (Figure S14).

To estimate how the different conformational repertoires of our TMD helices might predispose them for cleavage by presenilin, the respective structural bundles were superimposed onto the Notch1 TMD in the cryo-EM structure of its complex with γ-secretase (6IDF[38]). In that structure, the Notch1 residues L1755-L1756-S1757 close to the C-terminus form the tripartite β-sheet with presenilin. Formation of this sheet is thought to stabilize the partially unfolded state of the substrate TMD, as required for S3 cleavage. Here, we reasoned that a TMD conformation permitting cleavage might place its sheet-forming residues close to the site where it will join the strands from presenilin. To test this idea, we first aligned our average wt Notch1 structure (Figure S13) with the backbone atoms of the substrate helix in the cryo-EM structure. The other NMR models were superimposed

along their TM-N onto the wt structure thus obtained Figure 9. The Notch1 TMD bundle fits reasonably well into the space between the presenilin TMDs, although 12/40 structures of the bundle collide with presenilin TM7. Likewisely, the structural bundles of the Notch variants collide to various extents (Notch1 $L_{1740-1743}$, 17/40; Notch1 $G_{1740-1743}$, 23/40; Notch3, 23/40). In the bottom of Figure 9, we isolated presenilin TMDs 6 and 7 (harboring the catalytic Asp residues) and both β-strands contributed by presenilin to the tripartite β-sheet (marked in red). These crucial elements are overlaid with the locations of the C_α atoms of L1756, the central residue of the β-strand. In case of wt Notch1, most L1756 C_α atoms are indeed tightly clustered near the presenilin β-strands. The respective C_α ensembles of wt Notch3 and Notch1 $L_{1740-1743}$ are also clustered tightly; however, both clusters are more distant from the presenilin strands than the wt Notch1 cluster. In accord with the widely distributed conformations of Notch1 $G_{1740-1743}$ (Figure 8(d)), the C_α atoms of its L1756 occupy a large area that includes the C_α positions of the other TMD variants. It appears, therefore, as if the average spatial proximity between residues forming the tripartite β-sheet roughly matches the cleavability of the respective substrate variants.

To test the general applicability of this modeling approach, we performed a similar analysis using the structure of the APP-derived C83 fragment in complex with γ-secretase (6IYC[7]). Specifically, we compared the models of the wt APP TMD with those of two derivatives where mutation of the $V_{36}G_{37}G_{38}V_{39}$ hinge motif (G38L or G38P) had drastically reduced ε-cleavage in previous work.[53] Here, the structural bundles of the wt TMD also fit reasonably well into presenilin with minor clashes for 7/20 structures (Figure S15). By contrast, significant numbers of the models of G38L (9/20) and G38P (12/20) collide with presenilin, as noted previously.[20] As shown in the bottom of Figure S15, the C_α atoms of M51 of the wt APP TMD cluster near the presenilin β-strands. By contrast, with both mutants, the respective clusters of the few remaining models localized further away from the presenilin strands, consistent with their lower cleavabilities.

In sum, wt Notch1 departs more strongly from the canonical α-helical structure than the less cleavable Notch3. While the AAAA → LLLL mutant straightens the Notch1 helix, AAAA → GGGG introduces a very flexible site leading to great structural disorder. In the context of a modeled substrate/enzyme complex, the sheet-forming residues near the Notch1 C-terminus tend to localize closer to the site of the eventual tripartite sheet than those of the Notch3 and the Notch1 Leu mutant. A broader distribution of corresponding residues is seen with the Gly mutant, albeit associated with greater experimental uncertainty.

Discussion

In this study, we initially developed a novel yeast-based cleavage assay which differs from previous assays in several aspects. In one previous yeast system, the substrate is expressed from a genomically integrated reading frame while γ-secretase subunits are encoded episomally[32]; in another system, γ-secretase subunits and substrate are both episomally encoded.[34,54] In the system presented here, the multi-copy nature of the plasmid ensures an excess of substrate over γ-secretase, thus excluding substrate-limitation as a potentially rate-limiting factor in cleavage. Further, the fusion of substrate and GFP sequences allowed us to monitor substrate expression and revealed sorting to the vacuolar membrane of the cell, which is where cleavage is likely to take place.

A mutational screen revealed that replacing the AAAA or AGAV motifs within the TM-Ns of Notch1 or Notch3, respectively, by LLLL abolished cleavage. In keeping with the idea that the small side chains within the wt motifs confer cleavage-promoting helix flexibility, a GGGG motif significantly facilitated cleavage. DHX analysis of corresponding TMD peptides confirmed this expectation in revealing strong helix stabilization by LLLL and destabilization by GGGG. NMR spectroscopy uncovered a bent 3D structure of the Notch1 helix. Previous NMR analysis had found a rather straight Notch1 helix in mixed detergent/lipid bicelles.[27,28] Presumably, the bend detected by us forms only in a more polar solvent, such as 80% TFE which we used to mimic the polar interior of presenilin.[43,44] Higher polarity is likely to weaken amide H-bonds such that an accumulation of smaller amino acid side chains along one face of the helix relative to the other face can elicit bending. Consistent with this idea, the bend is diminished in the LLLL mutant. By contrast, GGGG introduces marked structural disorder and subdivides the TMD into two short independent helices. Consistent with a destabilizing effect of small side chains, the helix appears to be distorted at the AAAA motif of Notch1 bound to γ-secretase in the cryo-EM structure.[8] Our data are also consistent with a previous tudy where mutations A1740Y or A1741Y had slightly decreased S3 cleavage.[16] Analysis of pairwise sequence alignments uncovers VVAA or GAAA as consensus motifs at the site of the original AAAA or VAGA in Notch1 or Notch3, respectively.

How could the conformational flexibility of the Notch TM helix affect its cleavability by γ-secretase? A flexible TM helix may facilitate its translocation from the enzyme/membrane boundary to a cleavage-competent location where the S3 site can dock into the catalytic cleft, as proposed previously for the TM helix of the C99 fragment of APP.[18,53,55] For a better mechanistic insight, we approximated potential conformational states of wt Notch TMDs as well as the

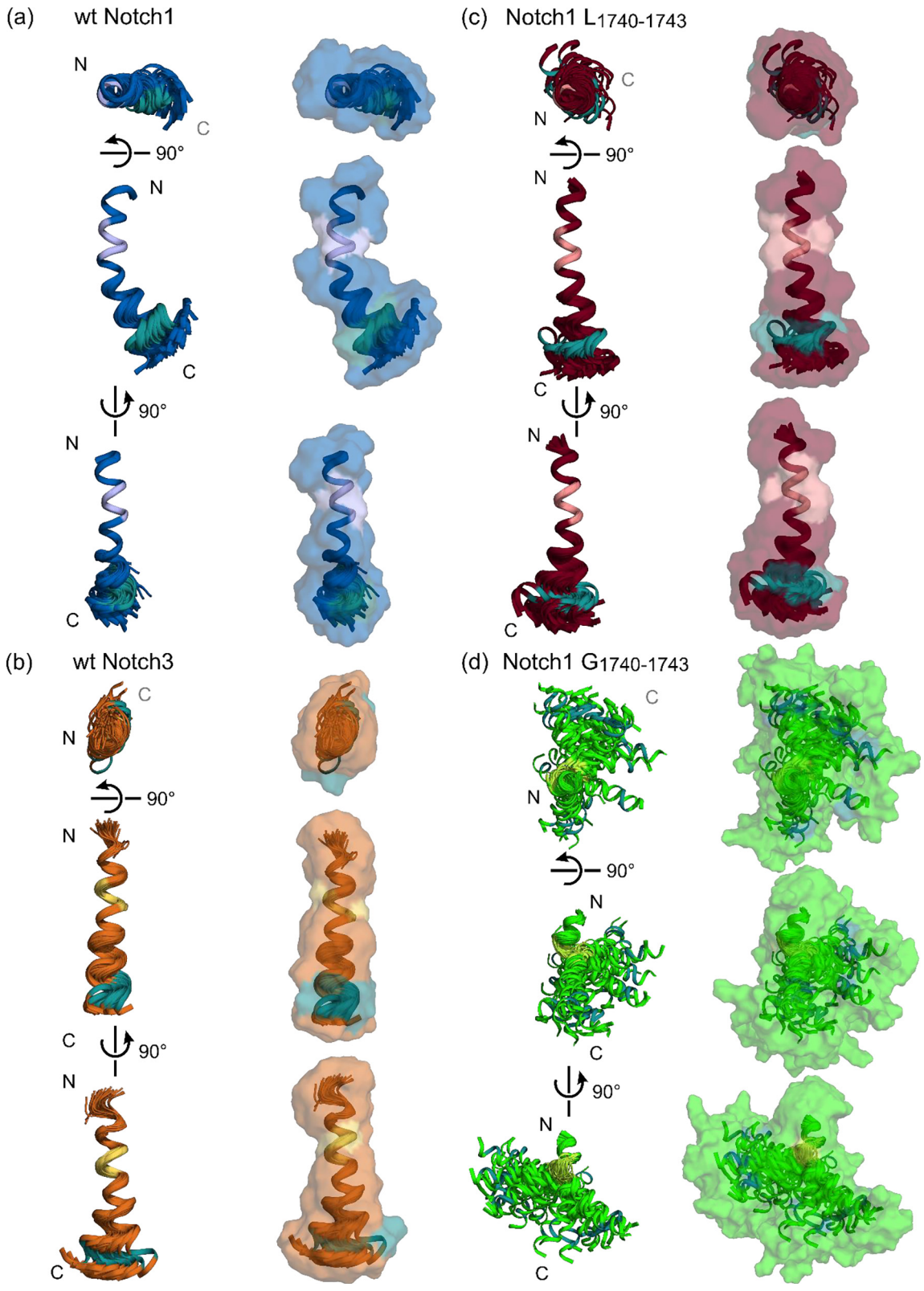

Figure 8. Structural bundles and surfaces characterizing substrate TMD 3D structures. (a)–(d) Structural bundles of wt Notch1 (a) and both mutants (c, d), superimposed at residues L1734-L1747 and wt Notch3 (b) aligned at L1644-I1657. Top and side views of the 40 lowest-energy NMR structures out of 400 are shown. On the left: bundles of helix backbone structures; on the right: backbone bundles surrounded by transparent surfaces corresponding to side chains. The Notch1 AAAA, LLLL, and GGGG motifs, as well as the AGAV motif of wt Notch3 are colored more lightly. S3 cleavage sites are marked in turquoise.

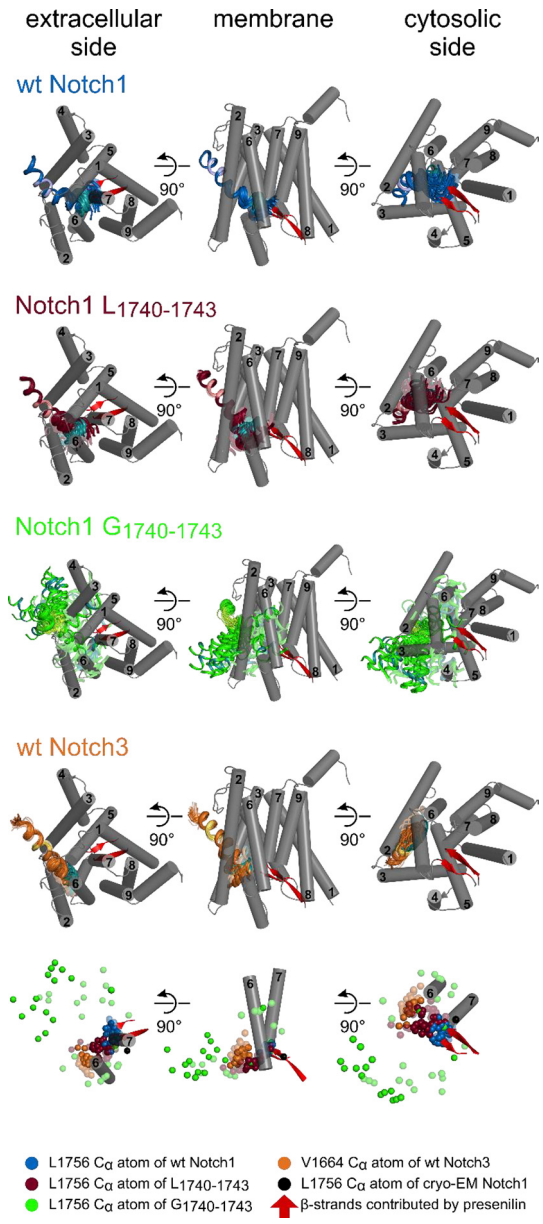

Figure 9. Structural models of Notch/enzyme complexes. Extracellular, membrane, and cytosolic views of putative substrate/enzyme structures. These structures were obtained by modelling the conformational repertoires of wt and mutant Notch TMDs into the experimental Notch1/γ-secretase cryo-EM structure (pdb code: 6IDF.[8] The Notch1 AAAA, LLLL, and GGGG motifs, as well as the AGAV motif of wt Notch3 are colored more lightly. S3 cleavage sites are represented in turquoise. Of the γ-secretase subunits, only presenilin (grey with numbered TMDs) is shown; its β-strands formed by residues between TMDs 6 and 7 and by the TMD7 N-terminus are highlighted in red. In the bottom, TMDs 6 and 7 plus the presenilin β-strands are isolated for improved clarity. Structures within a distance of <3 Å to presenilin TMDs and thus colliding with them are displayed in transparent mode. We maintained the colliding structures in order to visualize the full range of models.

AAAA → LLLL and AAAA → GGGG mutants within γ-secretase by aligning them with the structure of native Notch1 being part of the cryo-EM structure.[8] Although presenilin may constrain the dynamics of a substrate helix in ways different from TFE, we find that many potential conformers can exist within the enzyme without structural clashes. Interestingly, average proximities of those substrate residues that are to form the tripartite β-sheet with presenilin,[8] to the final location of the sheet roughly match the cleavabilities of the respective substrate variants. In other words, we propose that the AAAA/AGAV motifs are crucial in presenting the sheet-forming residues to the cognate presenilin domains. By influencing the rate of sheet formation, the AAAA/AGAV motifs are thus likely to influence the stability of the unfolded state around the S3 site. A similar picture emerged when we modeled the conformational ensembles of the APP TMD in its complex with γ-secretase. In this case, we compared two mutants of the well-characterized VGGV hinge to the wt TMD. Again, the greatly diminished cleavabilities of both mutants[53] roughly match the proximities of the sheet-forming residues in the modeled structures. We stress, however, that the APP TMD exhibits a well-defined hinge at its VGGV motif[19,20] whereas the wt Notch1 TMD forms a continuous helix with its characteristic bend. We also note that the sum of our data questions a simple link between cleavability and helix flexibility. First, Notch3 is cleaved with lower efficiency than Notch1 despite Notch3 displaying stronger TM-N flexibility, according to our DHX data. Second, analyzing our Notch1/Notch3 chimera showed TM-C to be more important than TM-N in transferring paralog-specific cleavability from Notch1 to Notch3 and *vice versa*. We thus propose that helix dynamics permitting cleavage appear to be defined by cooperating TM-N and TM-C domains. Further, the nature of conformational substates accessible to a given TMD, as revealed by NMR spectroscopy, is a more appropriate predictor of cleavability than mere H-bond strength along the helix backbone. In addition, domains outside the TMDs are likely to contribute to cleavability in ways yet to be analyzed. Juxtamembrane regions have previously been implied to affect cleavage of C99[56–58] and other substrates, including Notch.[59] Specifically, the Lys residue at the N-terminal border of the C99 TMD appears to interact with the gate-keeper subunit nicastrin, thus regulating the processivity of proteolysis.[5] Although no basic residue is present at the N-terminus of Notch1 and Notch3 TMDs, we cannot exclude that a Notch/nicastrin interaction is influenced by the conformational flexibility of the TMD.

The concept of cooperating TM-N and TM-C domains is supported by the pronounced mutational sensitivities of six to nine residues within the TM-C of both Notch paralogs. TM-C harbors domains essential for cleavage, including the S3 site. Point mutagenesis of Notch1 indeed showed G1753 and

V1754 bordering S3 to be among those residues being most important for cleavage. How does the structure of these amino acids facilitate bond scission? One intuitively appealing possibility is that these helix-destabilizing residues[47,60] promote local helix unfolding prior to cleavage. Indeed, it is well known that cleavage sites within substrates of soluble proteases are abundant in loop regions as well as in unstable helical regions.[61] One the one hand, a role of G1753 and V1754 in helix unfolding is supported by the slight reduction in helicity and structural order near this site, as indicated by our chemical shift data. Also, Pro mutations downstream of the initial APP cleavage sites have recently shown to facilitate cleavage.[54] On the other hand, several findings argue against this interpretation including that (i) none of our presumably helix-destabilizing Pro mutations around the S3 site promoted cleavage, (ii) exchanging V1754 by either Leu or Gly had previously strongly compromised cleavage,[17] and (iii) cleavage-promoting substitutions to Val downstream of S3 have no significant impact on H-bond strength close to the C-terminus where wt helix stability is already quite low. Therefore, we suggest that mutating G1753 and V1754 may interfere with tight docking of the unfolded substrate into the catalytic cleft of presenilin and/or the attraction of catalytic water[62,63] prior to bond scission. A similar conclusion had recently been reached by analyzing the APP TMD. There, an artificial GG motif introduced at the sites of initial cleavage had strongly increased helix flexibility but not its cleavage by γ-secretase.[18] Nonetheless, the wt sequence around these sites was found to cooperate with the more N-terminal VGGV hinge motif in rendering a poly-Leu template cleavable. In the present study, we also succeeded in designing artificial minimal substrate TMDs by grafting multiple sequence-optimized motifs derived from Notch1 onto polyLeu. The results identified TM-N and TM-C motifs as both being required for cleavage at the level of wt Notch1 or even above. Cooperation between different TMD segments for cleavability thus appears not to be restricted to the APP TMD with its pronounced hinge. That previous APP study had already proposed tight docking of the sequence around the initial cleavage site into the catalytic cleft as one potential constraint govering the evolution of cleavage sites. Our current results point to another function of the TM-C that might relate to the stability of the tripartite β-sheet with presenilin. We propose that our mutations to sheet-stabilizing Val[41] promote sheet formation, thus indirectly stabilizing the unfolded state around S3 for cleavage. Similar to both Notch paralogs, mutations to Val at the very C-terminus of the APP TMD also promoted its cleavage while Leu abolished it. In agreement with this hypothesis, negatively charged residues within the β-strand-forming sequence of the APP TMD facilitated its cleavage, possibly by way of artificial electrostatic interactions with K380 within the respective β-strand of presenilin.[54] Future studies will show to which extent sheet-promoting residues facilitate cleavage of other substrates and how stabilization of the tripartite sheet can be experimentally proven. Notably also, mutating one central residue within the β-strand of the substrate (Notch1 S1757 or Notch3 A1665) to Val did not promote cleavage and S1757 belongs to the most mutation-sensitive Notch1 residues overall. The structural role of these residues is currently unclear.

Conclusion

In terms of the structural properties enabling cleavage, the TMDs of Notch1 and several other intramembrane protease substrates exhibit commonalities as well as differences. Previously investigated cases with known NMR structures include TMDs of APP[19,20,53] and two substrates of the signal-peptide-peptidase-like protein, namely TNFα[64] and GnTV.[65] In all these cases, conformational flexibility of the helices is encoded by TM-N motifs containing Gly and/or Ala. It is becoming increasingly clear that cleavability depends on the ability of a TMD to adopt permissive conformational substates within the structural context of its cognate enzyme. The ability to adopt permissive conformations manifests itself as helix curvature in case of Notch1, TNFα, and GnTV TMDs, while an explicit hinge is formed by the APP TMD. Accumulations of Gly, Ala, and/or helix-destabilizing β-branched residues have previously also been detected at conformationally flexible regions within the TM-Ns of γ-secretase substrates ErbB4 and N-cadherin, suggesting that TM-N flexibility enhances their cleavability of other substrates, as well.[18] To which extent related motifs facilitate the cleavability of the plethora of known substrate TMDs[1] is currently unknown, however. Further, helix flexibility near the scissile bonds appears not to affect cleavability of the Notch1 TMD, in agreement with previous findings related to the APP[18] and TNFα TMDs.[64] Although cleavage requires an unfolded cleavage site, it is likely that helix unfolding around cleavage sites may not constitute a rate-limiting step in intramembrane proteolysis. Indeed, helices in aqueous solution unfold at nanosecond timescales.[12] This is orders of magnitude faster than notoriously slow intramembrane proteolysis[4,11,66] and thus unlikely to limit its rate. Finally, our data suggest that the cleavage-promoting impact of mutations to Val within the β-sheet-forming part of the TMDs of both Notch paralogs and C99 may rest on stabilization of the tripartite β-sheet in the substrate/enzyme complex, thus extending the life-time of the unfolded state required for cleavage.

Experimental Procedures

Construction of yeast strains for γ-secretase activity testing

To measure γ-secretase activity, novel yeast strains were constructed based on the commercial

Matchmaker Gold Yeast Two-Hybrid System (Clontech, order#630489). To this end, integrative shuttle vectors from the pRS40x vector series[67] were cloned. Bidirectional expression cassettes[68] containing the two promoter-terminator pairs GAPp / ADH1t and TEFp / CYC1t were cloned into the PvuII site of pRS402 and pRS405 using Gibson assembly according to manufacturer's recommendations (New England Biolabs, order# E2611S). Subsequently, frames of either nicastrin (UniProt ID Q92542 NICA_HUMAN, residues 1 to 709, GAP promoter) or APH-1a (UniProt ID Q96BI3 APH1A_HUMAN, residues 1 to 265, TEF promoter) carrying a C-terminal hemagglutinin (HA) epitope tag were cloned between EcoRI/SacI or BamHI/NheI sites into pRS402_GAPp/TEFp (resulting in pRS402-nicastrin/APH-1a-HA). In a similar manner, PEN2 (UniProt ID Q9NZ42 PEN2_HUMAN, residues 1 to 101, GAP promoter) carrying an N-terminal FLAG tag and presenilin 1 (UniProt ID P49768 PSN1_HUMAN, residues 1 to 467, TEF promoter) were cloned between the NotI/BglII or SalI/HindIII of vector pRS405_GAPp/TEFp (resulting in pRS405-FlagPEN2/PS1wt).

Yeast strains Y187 and Y2H Gold (both from Clontech) were used as basis for further genetic modifications. All yeast cells were transformed according to.[69] Initially, pRS402-nicastrin/APH-1a-HA was linearized with StuI and integrated into the ADE2-locus of strain Y187 resulting in the intermediate strain Y187_pRS402-nicastrin/APH-1a-HA. Integration was checked by auxotrophic selection on SC-Ade agar and PCR. pRS405-FlagPEN2/PS1wt was linearized with XcmI and integrated into the LEU2 loci of strains Y2H Gold as well as Y187_pRS402-nicastrin/APH-1a-HA. This resulted in the intermediate strain Y2HGold_pRS405-FlagPEN2/PS1wt and the novel strain GSY187 (GammaSecretaseY187). Integration into the respective genomes was checked by auxotrophic selection on SC-Leu (pRS405 only) or SC-Ade, -Leu (pRS402 and pRS405), and PCR. Strain MOY10 was constructed as a diploid between Y187_pRS402-nicastrin/APH-1a-HA and Y2HGold_pRS405-FlagPEN2/PS1wt. Both strains grown to a density of OD600 = 0.5 were combined and incubated in 15 mL 2xYPDA medium for 2 h at 30 °C. After two washes in H_2O, cells were plated on SC-Ade, -Leu agar and incubated for approximately 3 days at 30 °C. Diploid colonies were checked for cassette integration via PCR.

Construction of substrate fusion proteins

Fusion proteins composed of the invertase signal peptide (UniProt ID P00724 INV2_YEAST residues 1 to 19), 100-amino-acid-fragments of our candidate sequences of interest flanked by BglII and KpnI sites (e.g. Notch 1, Uniprot ID P46531 NOTC1_HUMAN, residues 1705 to 1804), superfolder-GFP (residues 1 to 236[70]) and full-lengh GAL4 (Uniprot ID P04386 GAL4_YEAST, residues 1-881) flanked by a C-terminal Strep-tag were expressed on a 2μ shuttle plasmid (derived from pGBKT7 DNA-BD Vector, Clontech #630443) under control of the TEF promoter.

Plasmids will be deposited at Addgene (https://www.addgene.org/).

Construction of a substrate mutant library

A substrate mutant library was constructed via a synthetic DNA oligonucleotide pool (Twist Biosciences, USA) that was cloned into our substrate vector. The oligonucleotide pool was amplified according to the manufacturer's recommendations using Q5 High Fidelity polymerase (New England Biolabs) with overhangs allowing for Golden Gate cloning using BsaI and T4 ligase (New England Biolabs). The recipient vector was prepared to harbor two BsaI cloning sites flanking a copy of the PPZ1 gene (Uniprot ID P26570 PPZ1_YEAST residues 1 to 692) with a 3′ stop codon as a placeholder within the Notch1 sequence allowing the transfer of the 150 bp PCR fragments encoding the intended point mutations. The recipient vector was predigested with BsaI and purified via agarose gel electrophoresis. DNA at a stoichiometric vector/insert ratio = 1:5 was incubated with BsaI and T4 ligase (5 min at 37 °C, 5 min at 16 °C; 30 cycles). After heat inactivation at 60 °C for 10 min, additional BsaI was added followed by incubation at 37 °C for 1 h. Assembly products were transformed into *E. coli* XL10 (Agilent) and cells were grown overnight in LB medium containing kanamycin (35 mg/mL). Plasmids were isolated using NucleoBond Xtra MIDI kit (Machery Nagel, Germany #740410).

Measuring substrate cleavage efficiency

Cleavage was measured as β-galactosidase (β Gal) activity that results from activation of the *lacZ* reporter gene in strain GSY187. The activation of *lacZ* was triggered by the GAL4p moiety being part of the intracellular fragment of a substrate fusion protein upon its release resulting from cleavage. Yeast strains GSY187 and Y187 were transformed with plasmids encoding our substrate fusion proteins and plated on SC-Trp agar to select for transformants. After 2–3 days of incubation at 30 °C, 6 mL SC-Trp medium was inoculated with approximately 10 colonies and incubated overnight at 30 °C using an orbital shaker (Infors AK82). Aliquots of 2 mL cells were subsequently washed two times by centrifuging (10,000 × *g* for 2 min) and resuspending in 2 mL fluorescence-free PBS (Gibco). Subsequently, 200 μL aliquots were transferred to a clear 96-well plate and OD660 was measured for cell density using a VersaMax plate reader (Molecular Devices). β Gal kinetics were measured using the yeast β-Galactosidase Assay Kit (ThermoFisher

#75768). Maximal velocities of β Gal production (vMax) were calculated from the slope of a line fitted to the kinetics data in SoftMax Pro v5.0.1 (Molecular Devices). Miller Units correspond to the ratio vMax/OD660.

For non-normalized data, statistical analysis was performed using one-way ANOVA paired with Tukey's post hoc tests. For comparing the β Gal activity of a wt reference protein to the activity of a corresponding mutant normalized to the wt, one-sample t-tests were used. Comparing two normalized β Gal activites was achieved by two-sample t-tests.

Expression levels of substrate constructs were assessed via fluorescence measurements of the intrinsic sfGFP. Initially, OD600 was measured in a 96-well format (Molecular Devices VersaMax). Thereafter, cells were transferred to a 96-well fluorescence plate (Thermo Scientific #237108) and fluorescence intensity (λ_{ex} = 485 nm, λ_{em} = 520 nm, bandwidth = 10 nm, BMG Polarstar Omega) was measured. Arbitrary fluorescence units correspond to the fluorescence/OD600 ratios. Mock controls lacking sfGFP were subtracted from arbitrary fluorescence units. For inhibitor studies, the γ-secretase Inhibitor LY-411,575, stored as 1 mM stock solution in DMSO, was added to the growth medium and γ-secretase activity was measured as described above.

Library based screening of Notch1 mutants

Alternative to measuring β Gal activity, cleavage was determined via competitive growth of a sequence library expressed in strain MOY10. The HIS3 reporter gene of MOY10 is under control of GAL4-responsive elements and thus activated by intracellular substrate fusion protein fragments released by cleavage. The library was transformed and plated on 140 mm petri dishes containing SC-Trp agar. After growth at 30 °C for approximately 48 h, all transformants were harvested from the agar plate and washed twice by centrifuging (10,000xg for 2 min) and resuspended in 10 mL H_2O. Approximately 1500 clones were plated onto 140 mm petri dishes containing either SC -Ade, -Leu, -Trp, -His Agar (OUT-pool, selective medium) or SC-Ade, -Leu, -Trp Agar (IN-pool, no selection). Cells were grown at 30 °C until the first colonies were visible (∼40 h). After all cells were harvested and washed as described above, plasmids were isolated via spin-column purification after treatment with zymolase (Machery-Nagel NucleoSpin Plasmid #740588, Zymo Research #E1005). The numbers of transformants surviving under selective conditions were determined by next-generation-sequencing (NGS). Amplicons for NGS were obtained by PCR using oligonucleotides designed to amplify a 300 bp substrate coding region in order to count surviving clones. Primers were equipped with 5′ universal sequencing adapters. Sequencing was done at Eurofins Genomics (Amplicon 2nd PCR, Illumina 2x300 bp paired end). NGS read counts were extracted from fastq files using custom python code. For each sequence, the read-count OUT-pool/IN-pool ratio was calculated and normalized to wt Notch1 set to 100%.

Confocal microscopy

Confocal microscopy was utilized to assess the subcellular distribution of selected substrate constructs. Transformed cells were grown in 6 mL SC-Trp or YPDA overnight, diluted to an OD600 = 0.2–0.3 and re-grown up to OD600 = 1. Log-phase cells were directly mounted to glass slides and analyzed via confocal imaging using a Leica TCS SP8 X WLL2 upright Hyvolution 2 (λ_{ex} 488 nm, λ_{em} 493−650 nm). Image Z-Stacks were recorded in 0.3 nm steps and a representative frame with best focus was chosen for visualization. Images were processed in Leica's Application Suite X (ver. 3.7.4.23463). Control cells harbor GFP-tagged Vph1 (a marker for vacuolar localization) or Zeo1 (plasma membrane localization).

BLAST analysis

C100, Notch1-100, and Notch3-100 were blasted against UniRef90. All pairwise sequence alignments were analyzed using a custom python script. Only sequences with a minimal homology of 40% and a maximum of 5 gaps within the TMD were assumed as valid. The minimal allowed homology within the full-length sequence was set to 50%. All match sequence TMDs were aligned using the query TMD as scaffold. Amino acid conservations from all matched sequences were calculated for each aligned position and the consensus sequence was constructed from the most abundant amino acid at each position.

Peptide synthesis

Peptides were synthesized by Fmoc chemistry by PSL, Heidelberg, Germany and purified to >90% purity as judged by mass spectrometry. All other chemicals were purchased from Sigma-Aldrich Co. (St. Louis, Missouri, USA).

Deuterium-hydrogen exchange

Synthetic peptides were exhaustively (>95%) deuterated prior to DHX. The peptide solutions (100 μM in 80% (v/v) d1-trifluoroethanol (d1-TFE) in 2 mM ND_4-acetate and 1 mM deuterated DTT) were then diluted 1:20 with protonated 80% (v/v) TFE, 2 mM NH_4-acetate, 0,5 mM Tris(2-carboxye thyl)phosphinhydrochlorid, pH 5.0 (except for Notch1 mutant $G_{1740-1743}$ which was measured at pH 4.0) and incubated at 20.0 °C. Exchange reactions were quenched after different periods of

time by cooling on ice and lowering the pH to 2.5 by adding 0.5% (v/v) formic acid. Mass spectrometry was performed on a Synapt G2 HDMS (Waters Co., Milford, MA) and measurements were taken from distinct samples. Samples were injected from a 100 μL Hamilton gas-tight syringe via a Harvard Apparatus 11 Plus with a flow rate of 5 μL/min. Spectra were acquired in a positive-ion mode with one scan per second and a 0.1 s interscan time. Mass/charge ratios were recorded and evaluated as previously described.[71] For electron transfer dissociation (ETD), we used 1,4-dicyanobenzene as an electron donor and preselected 5+ charged peptides via MS/MS. Fragmentation of peptides was performed as described.[26] Briefly, ETD MS/MS scans were accumulated over a 10 min scan time. ETD-measurements were performed after 13 different incubation periods (from 1 min to 3 d) where exchange had taken place at pH 5.0. We note that base-catalyzed exchange is responsible for at least 95% of the total deuteron exchange at pH $\geq$ 4.0. The resulting ETD c' and z fragment spectra were evaluated using a semi-automated procedure (ETD FRAGMENT ANALYZER module of MassMap-deutsch-2022-05-21 Software.[18,42] As noted previously,[18] the exchange kinetics of the wt Notch1 TMD exhibit a biphasic shape near both helix termini as well as at some internal positions. Similarly biphasic DHX was also seen at various positions within the Notch1 mutants and within Notch3 (Figure S8(a)). It is assumed that the fast phase reflects a superposition of reactions in a mixed regime of correlated (EX1) and uncorrelated (EX2) exchange[72,73] while the slow phase results from EX2 only (see Supplemental Note 1 in.[18] During uncorrelated EX2 exchange, H-bond formation after local unfolding is much more rapid than DHX; which permits determination of the ΔG values[74] from the slow phase of the respective kinetics.

Monoexponential fitting of the data was done with equation (1) to calculate $k_{exp,DHX}$, which accounts for the concentration of deuterated solution in the DHX-ETD assay of 5% (v/v)

$$D(t) = 0.95 \cdot e^{-k_{exp}t} + 0.05 \quad (1)$$

while biexponential fitting was done with equation (2):

$$D(t) = A \cdot e^{-k_{exp,A}t} + B \cdot e^{-k_{exp,b}t} + 0.05 \quad (2)$$

Where A and B are the population sizes of the deuterons with slower and faster exchange rates, $k_{exp,A}$ and $k_{exp,B}$, respectively, and A + B = 0.95. The decision between applying a mono- or biexponential fitting routine was based on Wilks' theorem using a p-value of 0.01 for monophasic behavior to assign biphasic ($p < 0.01$) or monophasic ($p > 0.01$) behaviour, as described.[18] Table S2 lists exchange rate constants and respective population sizes.

The free energies ΔG required for H-bond opening were calculated from k_{exp} (monophasic DHX) or $k_{exp,B}$ (the smaller rate constant in cases of biphasic DHX) and k_{ch} based on equation (3) based on Linderstrøm-Lang theory,[74] assuming EX2 conditions and a predominantly folded state[18,42]

$$\Delta G = -R\,T\ln\left(\frac{k_{exp,DHX}}{k_{ch} - k_{exp,DHX}}\right) \quad (3)$$

where k_{ch} represents the sequence-specific chemical rate constants that were calculated using the program SPHERE (https://landing.foxchase.org/research/labs/roder/sphere/) (under the set conditions: D-to-H-exchange, reduced Cys, pH = 5.0, T = 20.0 °C). We note that, for potential reasons outlined in the Supplemental Note 1 of ref.[18], our calculated ΔG values might be underestimating the true values to some extent.

Statistics – Mass spectrometry

Residue-specific DHX kinetics (equations (2) and (3)) originate from time-dependent deuteron contents D_{mean} averaged from the masses of different fragment ions. The residue-specific D_{mean} values were obtained from raw MS data after applying a smoothing function by the MassMap® software to the D contents of series of c- and z-fragments produced by ETD at the different time points. As a result of the smoothing procedure, the precision of the deuteron contents is significantly improved. Rate constants $k_{exp,DHX}$ were determined by a non-linear least squares fitting routine. Standard errors of $\log k_{exp,DHX}$ result from the errors of the fits. The limits of the standard confidence interval of ΔG are calculated by means of the standard error of $\log k_{exp,DHX}$. A detailed account of the procedure is presented in the manual associated with the computer code at https://doi.org/10.5281/zenodo.7223537.

NMR spectroscopy

Peptides used were identical to those used for DHX (Table S1). Dry peptides were dissolved in hexafluorisopropanol and H_2O (80:20, v:v), 1 mM Tris(2-carboxyethyl)phosphinhydrochlorid was added to reduce potential disulphide bridges and pH was adjusted to between 4 and 5 by adding NaOH. The solvent was removed by lyophilisation and the dry peptide film was dissolved in 500 μL d2-trifluorethanol (d2-TFE) and H_2O (80:20, v:v) with renewed addition of Tris(2-carboxyethyl)phosphinhydrochlorid to a final concentration of 1 mM. The pH was finally adjusted to 6.5 and peptide concentration ranged between 2 and 4 mg/mL (500 μM and 1 mM).

NMR spectra were recorded on a 600 MHz Avance III spectrometer (Bruker BioSpin, Rheinstetten, Germany) equipped with a TCI cryoprobe at a temperature of 300 K. To assign ^{1}H, ^{13}C and ^{15}N resonances of the peptides homonuclear $^{1}H^{1}H$-TOCSY (mixing time 60 ms),

$^{1}H^{1}H$-NOESY (mixing time 200 ms) and natural abundance $^{1}H^{13}C$-heteronuclear single quantum coherence (HSQC) and $^{1}H^{15}N$ HSQC spectra were acquired. For acquisition and spectral processing, TopSpin (Bruker, BioSpin, Rheinstetten, Germany) was used.

CcpNmr Analysis[75] was used for assignment of resonances and integration of NOE peaks. Secondary chemical shifts were determined as the difference between observed and random coil values.[48] To account for the influence of neighbouring amino acids on the chemical shift, a nearest neighbour correction[48] was applied. Dihedral restraints for Φ and Ψ backbone dihedral angle, S^2 order parameters and helix probability were derived from chemical shift data using the program TALOS+.[52] All structure calculations were performed with CNS[76] using the ARIA2 setup[77] based on dihedral restraints and distance restraints derived from NOESY peak intensities. Table S3 lists structure statistics. PyMOL (The PyMOL Molecular Graphics System, Version 2.3.1, Schrödinger, LLC) was used to visualize the protein structures.

Structural alignment

The structural alignment of NMR structures was accomplished using PyMOL. The deflection of the individual structures within the wt Notch1 bundles was shown by superimposing 40 lowest-energy NMR structures onto the average wt Notch1 structure along the TM-N residues L1734-L1747. To compare the mutant structural bundles to those of wt Notch1, first the average Notch1 $L_{1740\text{-}1743}$ structure was aligned with the average wt Notch1 TM-N L1734-L1747 and then the remaining lowest-energy Notch1 $L_{1740\text{-}1743}$ NMR models were superimposed onto its Notch1 $L_{1740\text{-}1743}$ average structure along L1734-L1747. In case of Notch1 $G_{1740\text{-}1743}$ the average structure was first aligned along the backbone atoms of the entire TMD (L1734-S1757) with the wt Notch1 average structure and then the remaining Notch1 $G_{1740\text{-}1743}$ NMR models were superimposed onto its average structure along TM-N (L1734-V1745). An average structure of wt Notch3 was aligned with the backbone atoms of residues L1644-I1657 along the average wt Notch1 structure. The lowest-energy NMR models of wt Notch3 were aligned onto its average structure along TM-N (L1644-I1657).

The structural bundle of the wt Notch1 TMD investigated here was visualized within the ezyme-substrate complex by superimposing it onto the original Notch1 TMD within the cryo-EM structure (6IDF[8]). To this end, the average wt Notch1 structure from NMR was aligned with the backbone atoms of the entire helix L1743-S1757 of the cryo-EM Notch1 TMD; all other NMR models were superimposed onto the average wt Notch1 structure as described above. The structural bundle of the wt APP TMD (6YHF[20]) was visualized within the ezyme-substrate complex by superimposing it onto the original APP TMD within the cryo-EM structure (6IYC[7]). To this end, the average wt APP structure from NMR was aligned with the backbone atoms G29-G38 of TM-N of the cryo-EM APP TM-N; all other NMR models were superimposed onto the average wt APP structure along G29-G38 of TM-N. Distances of less than 3 Å between heavy backbone atoms of NMR structures and presenilin TMDs were determined with a PyMOL plugin python script (https://wiki.pymol.org/index.php/Show_contacts).

Author Contributions

MO, development of yeast system, cleavage assays, and microscopy; NGS, NMR spectroscopy and data evaluation as well as model building; WS, DHX assays; CMG, funding aquisition, supervision of NMR experiments and model building; DL, funding aquisition, design and supervision of cleavage assays and DHX analysis. DL wrote the manuscript together with the co-authors. All authors analysed their data, created their figures and have given approval to the final version of the manuscript.

Additional Information

Supporting information contains Tables S1, S2, S3 and Figures S1 – S15.

Data Availability

The atomic coordinates and experimental data have been deposited in the Protein Data Bank PDB (www.pdb.org) and Biological Magnetic Resonance Bank BMRB (https://bmrb.io/). wt Notch1 (PDB ID: 8OR5; BMRB ID: 34804), Notch1 $L_{1740\text{-}1743}$ (PDB ID: 8ORY; BMRB ID: 34806), Notch1 $G_{1740\text{-}1743}$ (PDB ID: 8ORZ; BMRB ID: 34807), wt Notch3 (PDB ID: 8OS0; BMRB ID: 34808).

DECLARATION OF COMPETING INTEREST

The authors declare that they have no known competing financial interests or personal relationships that could have appeared to influence the work reported in this paper.

Acknowledgements

We thank Drs. Ayelen Gonzalez Montoro and Christian Ungermann for helpful advice with yeast genetics and microscopy as well as for providing plasmids and yeast strains used to visualize different membranes. We are grateful to Dr. Harald Steiner for useful advice. We also thank Doreen Tetzlaff for expert technical

assistance and the TUM Center for Advanced Light Microscopy (CALM) for providing the resources used for microscopy. This work was funded by the Deutsche Forschungsgemeinschaft (DFG, German Research Foundation) 263531414/FOR 2290 (CMG and DL). CMG thanks the HGF program Information (43.35.02) for financial support.

Appendix A. Supplementary data

Supplementary data to this article can be found online at https://doi.org/10.1016/j.jmb.2023.168218.

Received 28 April 2023;
Accepted 26 July 2023;
Available online 1 August 2023

Keywords:
cleavage;
notch;
conformational dynamics;
transmembrane domain

† These authors contributed equally.

Abbreviations:
APH-1, anterior pharynx defective protein; APP, amyloid precursor protein; βGal, β-galactosidase; cryo-EM, cryo-electron microscopy; DHX, deuterium/hydrogen-exchange; ETD, electron transfer dissociation; NOE, nuclear Overhauser effect; PEN-2, presenilin enhancer 2; sfGFP, superfolder green fluorescence protein; TMD, transmembrane domain; TFE, trifluoroethanol

References

1. Guner, G., Lichtenthaler, S.F., (2020). The substrate repertoire of gamma-secretase/presenilin. *Semin. Cell Dev. Biol.* **105**, 27–42.
2. Wolfe, M.S., (2012). Processive proteolysis by gamma-secretase and the mechanism of Alzheimer's disease. *Biol. Chem.* **393**, 899–905.
3. Steiner, H., Fukumori, A., Tagami, S., Okochi, M., (2018). Making the final cut: pathogenic amyloid-β peptide generation by γ-secretase. *Cell Stress* **2**, 292–310.
4. Bolduc, D.M., Montagna, D.R., Gu, Y., Selkoe, D.J., Wolfe, M.S., (2016). Nicastrin functions to sterically hinder gamma-secretase-substrate interactions driven by substrate transmembrane domain. *PNAS* **113**, E509–E518.
5. Petit, D., Hitzenberger, M., Lismont, S., Zoltowska, K.M., Ryan, N.S., Mercken, M., et al., (2019). Extracellular interface between APP and Nicastrin regulates Aβ length and response to γ-secretase modulators. *EMBO J.* **38**, 1–18.
6. Hardy, J., Selkoe, D.J., (2002). The amyloid hypothesis of Alzheimer's disease: progress and problems on the road to therapeutics. *Science* **297**, 353–356.
7. Zhou, R., Yang, G., Guo, X., Zhou, Q., Lei, J., Shi, Y., (2019). Recognition of the amyloid precursor protein by human gamma-secretase. *Science* **363**, eaaw0930
8. Yang, G., Zhou, R., Zhou, Q., Guo, X., Yan, C., Ke, M., et al., (2019). Structural basis of Notch recognition by human γ-secretase. *Nature* **565**, 192–197.
9. Kopan, R., Ilagan, M.X., (2009). The canonical Notch signaling pathway: unfolding the activation mechanism. *Cell* **137**, 216–233.
10. De Strooper, B., Annaert, W., Cupers, P., Saftig, P., Craessaerts, K., Mumm, J.S., et al., (1999). A presenilin-1-dependent gamma-secretase-like protease mediates release of Notch intracellular domain. *Nature* **398**, 518–522.
11. Kamp, F., Winkler, E., Trambauer, J., Ebke, A., Fluhrer, R., Steiner, H., (2015). Intramembrane proteolysis of beta-amyloid precursor protein by gamma-secretase is an unusually slow process. *Biophys. J.* **108**, 1229–1237.
12. Jesus, C.S.H., Cruz, P.F., Arnaut, L.G., Brito, R.M.M., Serpa, C., (2018). One peptide reveals the two faces of alpha-helix unfolding-folding dynamics. *J. Phys. Chem. B* **122**, 3790–3800.
13. Kwok, J.B., Li, Q.X., Hallupp, M., Whyte, S., Ames, D., Beyreuther, K., et al., (2000). Novel Leu723Pro amyloid precursor protein mutation increases amyloid beta42(43) peptide levels and induces apoptosis. *Ann. Neurol.* **47**, 249–253.
14. Bocharov, E.V., Nadezhdin, K.D., Urban, A.S., Volynsky, P.E., Pavlov, K.V., Efremov, R.G., et al., (2019). Familial L723P mutation can shift the distribution between the alternative APP transmembrane domain cleavage cascades by local unfolding of the e-cleavage site suggesting a straightforward mechanism of Alzheimer's disease pathogenesis. *ACS Chem. Biol.* **14**, 1573–1582.
15. Fernandez, M.A., Biette, K.M., Dolios, G., Seth, D., Wang, R., Wolfe, M.S., (2016). Transmembrane substrate determinants for gamma-secretase processing of APP CTFbeta. *Biochemistry* **55**, 5675–5688.
16. Xu, T.H., Yan, Y., Kang, Y., Jiang, Y., Melcher, K., Xu, H. E., (2016). Alzheimer's disease-associated mutations increase amyloid precursor protein resistance to gamma-secretase cleavage and the Abeta42/Abeta40 ratio. *Cell Discovery* **2**, 16026.
17. Vooijs, M., Schroeter, E.H., Pan, Y., Blandford, M., Kopan, R., (2004). Ectodomain shedding and intramembrane cleavage of mammalian notch proteins are not regulated through oligomerization. *J. Biol. Chem.* **279**, 50864–50873.
18. Werner, N.T., Hogel, P., Guner, G., Stelzer, W., Wozny, M., Assfalg, M., et al., (2023). Cooperation of N- and C-terminal substrate transmembrane domain segments in intramembrane proteolysis by gamma-secretase. *Commun. Biol.* **6**, 177.
19. Barrett, P.J., Song, Y., Van Horn, W.D., Hustedt, E.J., Schafer, J.M., Hadziselimovic, A., et al., (2012). The amyloid precursor protein has a flexible transmembrane domain and binds cholesterol. *Science* **336**, 1168–1171.
20. Silber, M., Hitzenberger, M., Zacharias, M., Muhle-Goll, C., (2020). Altered hinge conformations in APP transmembrane helix mutants may affect enzyme-substrate interactions of gamma-secretase. *ACS Chem. Nerosci.* **11**, 4426–4433.
21. Götz, A., Hogel, P., Silber, M., Chaitoglou, I., Luy, B., Muhle-Goll, C., et al., (2019). Increased H-bond stability relates to altered epsilon-cleavage efficiency and abeta levels in the I45T Familial Alzheimer's disease mutant of APP. *Sci. Rep.* **9**, 5321.

22. Götz, A., Mylonas, N., Högel, P., Silber, M., Heinel, H., Menig, S., et al., (2019). Modulating hinge flexibility in the APP transmembrane domain alters γ-secretase cleavage. *Biophys. J.* **116**, 2103–2120.
23. Langosch, D., Scharnagl, C., Steiner, H., Lemberg, M.K., (2015). Understanding intramembrane proteolysis: from protein dynamics to reaction kinetics. *Trends Biochem. Sci* **40**, 318–327.
24. Langosch, D., Steiner, H., (2017). Substrate processing in intramembrane proteolysis by gamma-secretase – the role of protein dynamics. *Biol. Chem.* **398**, 441–453.
25. Hitzenberger, M., Gotz, A., Menig, S., Brunschweiger, B., Zacharias, M., Scharnagl, C., (2020). The dynamics of gamma-secretase and its substrates. *Semin. Cell Dev. Biol.* **105**, 86–101.
26. Stelzer, W., Scharnag, C., Leurs, U., Rand, K.D., Langosch, D., (2016). The impact of the 'Austrian' mutation of the amyloid precursor protein transmembrane helix is communicated to the hinge region. *Chem. Select* **1**, 4408–4412.
27. Deatherage, C.L., Lu, Z.W., Kroncke, B.M., Ma, S., Smith, J.A., Voehler, M.W., et al., (2017). Structural and biochemical differences between the Notch and the amyloid precursor protein transmembrane domains. *Sci. Adv.*, 3.
28. Deatherage, C.L., Lu, Z., Kim, J.-H., Sanders, C.R., (2015). Notch transmembrane domain: secondary structure and topology. *Biochemistry* **54**, 3565–3568.
29. Stelzer, W., Langosch, D., (2019). Conformationally flexible sites within the transmembrane helices of amyloid precursor protein and Notch1 receptor. *Biochemistry* **58**, 3065–3068.
30. Okochi, M., Fukumori, A., Jiang, J., Itoh, N., Kimura, R., Steiner, H., et al., (2006). Secretion of the Notch-1 Abeta-like peptide during notch signaling. *J. Biol. Chem.* **281**, 7890–7898.
31. Tanii, H., Jiang, J., Fukumori, A., Tagami, S., Okazaki, Y., Okochi, M., et al., (2006). Effect of valine on the efficiency and precision at S4 cleavage of the Notch-1 transmembrane domain. *J. Neurosci. Res.* **84**, 918–925.
32. Edbauer, D., Winkler, E., Regula, J.T., Pesold, B., Steiner, H., Haass, C., (2003). Reconstitution of γ-secretase activity. *Nature Cell Biol.* **5**, 486–488.
33. Ran, Y., Hossain, F., Pannuti, A., Lessard, C.B., Ladd, G. Z., Jung, J.I., et al., (2017). gamma-Secretase inhibitors in cancer clinical trials are pharmacologically and functionally distinct. *EMBO Mol. Med.* **9**, 950–966.
34. Yonemura, Y., Futai, E., Yagishita, S., Suo, S., Tomita, T., Iwatsubo, T., et al., (2011). Comparison of presenilin 1 and presenilin 2 γ-secretase activities using a yeast reconstitution system. *J. Biol. Chem.* **286**, 44569–44575.
35. Steiner, H., Duff, K., Capell, A., Romig, H., Grim, M.G., Lincoln, S., et al., (1999). A loss of function mutation of presenilin-2 interferes with amyloid β-peptide production and Notch signaling. *J. Biol. Chem.* **274**, 28669–28673.
36. Wong, G.T., Manfra, D., Poulet, F.M., Zhang, Q., Josien, H., Bara, T., et al., (2004). Chronic treatment with the gamma-secretase inhibitor LY-411,575 inhibits beta-amyloid peptide production and alters lymphopoiesis and intestinal cell differentiation. *J. Biol. Chem.* **279**, 12876–12882.
37. Lessard, C.B., Rodriguez, E., Ladd, T.B., Minter, L.M., Osborne, B.A., Miele, L., et al., (2019). Individual and combined presenilin 1 and 2 knockouts reveal that both have highly overlapping functions in HEK293T cells. *J. Biol. Chem.* **294**, 11276–11285.
38. Yang, G., Zhou, R., Zhou, Q., Guo, X., Yan, C., Ke, M., et al., (2019). Structural basis of Notch recognition by human gamma-secretase. *Nature* **565**, 192–197.
39. Aurora, R. et al, (1994). Rules for a-helix termination by glycine. *Nature* **264**, 1126–1129.
40. Cordes, F.S., Bright, J.N., Sansom, M.S., (2002). Proline-induced distortions of transmembrane helices. *J. Mol. Biol.* **323**, 951–960.
41. Street, A.G., Mayo, S.L., (1999). Intrinsic ß-sheet propensities result from van der Waals interactions between side chains and the local backbone. *PNAS* **96**, 9074–9076.
42. Yucel, S.S., Stelzer, W., Lorenzoni, A., Wozny, M., Langosch, D., Lemberg, M.K., (2019). The metastable XBP1u transmembrane domain defines determinants for intramembrane proteolysis by signal peptide peptidase. *Cell Rep.* **26**, 3087–3099.
43. Schutz, C.N., Warshel, A., (2001). What are the dielectric "constants" of proteins and how to validate electrostatic models? *Proteins* **44**, 400–417.
44. Tolia, A., Chavez-Gutierrez, L., De Strooper, B., (2006). Contribution of presenilin transmembrane domains 6 and 7 to a water-containing cavity in the gamma-secretase complex. *J. Biol. Chem.* **281**, 27633–27642.
45. Doig, A.J., Errington, N., Iqbalsyah, T.M., (2005). Stability and design of alpha-helices. In: Buchner, K. (Ed.), *Handbook of Protein Folding*. Wiley, Weinheim, pp. 247–313.
46. Quint, S., Widmaier, S., Minde, D., Langosch, D., Scharnagl, C., (2010). Residue-specific side-chain packing determines backbone dynamics of transmembrane model helices. *Biophys. J.* **99**, 2541–2549.
47. Hogel, P., Gotz, A., Kuhne, F., Ebert, M., Stelzer, W., Rand, K.D., et al., (2018). Glycine perturbs local and global conformational flexibility of a transmembrane helix. *Biochemistry* **57**, 1326–1337.
48. Wishart, D.S., (2011). Interpreting protein chemical shift data. *Prog. Nucl. Magn. Reson. Spectrosc.* **58**, 62–87.
49. Wüthrich, K., (1986). NMR of Proteins and Nucleic Acids. Wiley, New York.
50. Wuthrich, K., Spitzfaden, C., Memmert, K., Widmer, H., Wider, G., (1991). Protein secondary structure determination by NMR. Application with recombinant human cyclophilin. *FEBS Letter* **285**, 237–247.
51. Wagner, G., Neuhaus, D., Worgotter, E., Vasak, M., Kagi, J.H., Wuthrich, K., (1986). Nuclear magnetic resonance identification of "half-turn" and 3(10)-helix secondary structure in rabbit liver metallothionein-2. *J. Mol. Biol.* **187**, 131–135.
52. Shen, Y., Delaglio, F., Cornilescu, G., Bax, A., (2009). TALOS+: a hybrid method for predicting protein backbone torsion angles from NMR chemical shifts. *J. Biomol. NMR* **44**, 213–223.
53. Gotz, A., Mylonas, N., Högel, P., Silber, M., Heinel, H., Menig, S., et al., (2019). Modulating hinge flexibility in the APP transmembrane domain alters γ-secretase cleavage. *Biophys. J.* **116**, 1–18.
54. Suzuki, R., Takahashi, H., Yoshida, C., Hidaka, M., Ogawa, T., Futai, E., (2023). Specific mutations near the amyloid precursor protein cleavage site increase gamma-secretase sensitivity and modulate amyloid-beta production. *Int. J. Mol. Sci.* **24**

55. Scharnagl, C., Pester, O., Hornburg, P., Hornburg, D., Götz, A., Langosch, D., (2014). Side-chain to main-chain hydrogen bonding controls the intrinsic backbone dynamics of the amyloid precursor protein transmembrane helix. *Biophys. J .* **106**, 1318–1326.
56. Ren, Z., Schenk, D., Basi, G.S., Shapiro, I.P., (2007). Amyloid beta-protein precursor juxtamembrane domain regulates specificity of gamma-secretase-dependent cleavages. *J. Biol. Chem.* **282**, 35350–35360.
57. Clemente, N., Abdine, A., Ubarretxena-Belandia, I., Wang, C., (2018). Coupled transmembrane substrate docking and helical unwinding in intramembrane proteolysis of amyloid precursor protein. *Sci. Rep.* **8**, 12411.
58. Tian, Y., Bassit, B., Chau, D., Li, Y.M., (2010). An APP inhibitory domain containing the Flemish mutation residue modulates gamma-secretase activity for Abeta production. *Nature Struct. Mol. Biol.* **17**, 151–158.
59. Zhu, I., Liu, R., Garcia, J.M., Hyrenius-Wittsten, A., Piraner, D.I., Alavi, J., et al., (2022). Modular design of synthetic receptors for programmed gene regulation in cell therapies. *Cell* **185** (1431–43), e16.
60. Quint, S., Widmaier, S., Minde, D., Hornburg, D., Langosch, D., Scharnagl, C., (2010). Residue-specific side-chain packing determines the backbone dynamics of transmembrane model helices. *Biophys. J.* **99**, 2541–2549.
61. Belushkin, A.A., Vinogradov, D.V., Gelfand, M.S., Osterman, A.L., Cieplak, P., Kazanov, M.D., (2014). Sequence-derived structural features driving proteolytic processing. *Proteomics* **14**, 42–50.
62. Dehury, B., Tang, N., Mehra, R., Blundell, T.L., Kepp, K.P., (2020). Side-by-side comparison of Notch- and C83 binding to γ-secretase in a complete membrane model at physiological temperature. *RSC Adv.* **10**, 31215–31232.
63. Chen, S.Y., Zacharias, M., (2022). An internal docking site stabilizes substrate binding to gamma-secretase: analysis by molecular dynamics simulations. *Biophys. J .* **121**, 2330–2344.
64. Spitz, C., Schlosser, C., Guschtschin-Schmidt, N., Stelzer, W., Menig, S., Gotz, A., et al., (2020). Non-canonical shedding of TNF alpha by SPPL2a Is determined by the conformational flexibility of its transmembrane helix. *Iscience.*, 23.
65. Papadopoulou, A.A., Stelzer, W., Silber, M., Schlosser, C., Spitz, C., Haug-Kroper, M., et al., (2022). Helical stability of the GnTV transmembrane domain impacts on SPPL3 dependent cleavage. *Sci. Rep.* **12**, 20987.
66. Dickey, S.W., Baker, R.P., Cho, S., Urban, S., (2013). Proteolysis inside the membrane is a rate-governed reaction not driven by substrate affinity. *Cell* **155**, 1270–1281.
67. Brachmann, C.B., Davies, A., Cost, G.J., Caputo, E., Li, J., Hieter, P., et al., (1998). Designer deletion strains derived from Saccharomyces cerevisiae S288C: a useful set of strains and plasmids for PCR-mediated gene disruption and other applications. *Yeast* **14**, 115–132.
68. Amen, T., Kaganovich, D., (2017). Integrative modules for efficient genome engineering in yeast. *Microb Cell.* **4**, 182–190.
69. Gietz, R.D., Schiestl, R.H., (2007). Frozen competent yeast cells that can be transformed with high efficiency using the LiAc/SS carrier DNA/PEG method. *Nature Protoc.* **2**, 1–4.
70. Pedelacq, J.D., Cabantous, S., Tran, T., Terwilliger, T.C., Waldo, G.S., (2006). Engineering and characterization of a superfolder green fluorescent protein. *Nature Biotechnol.* **24**, 79–88.
71. Stelzer, W., Poschner, B.C., Stalz, H., Heck, A.J., Langosch, D., (2008). Sequence-specific conformational flexibility of SNARE transmembrane helices probed by hydrogen/deuterium exchange. *Biophys. J.* **95**, 1326–1330.
72. Qian, H., Chan, S.I., (1999). Hydrogen exchange kinetics of proteins in denaturants: a generalized two-process model. *J. Mol. Biol.* **286**, 607–616.
73. Xiao, H., Hoerner, J.K., Eyles, S.J., Dobo, A., Voigtman, E., Mel'Cuk, A.I., et al., (2005). Mapping protein engergy landscapes with amide hydrogen exchange and mass spectrometry: I. A generalized model for a two-state protein and comparison with experiment. *Prot Sci.* **14**, 543–557.
74. Zheng, J., Strutzenberg, T., Pascal, B.D., Griffin, P.R., (2019). Protein dynamics and conformational changes explored by hydrogen/deuterium exchange mass spectrometry. *Curr. Opin. Struct. Biol.* **58**, 305–313.
75. Vranken, W.F., Boucher, W., Stevens, T.J., Fogh, R.H., Pajon, A., Llinas, M., et al., (2005). The CCPN data model for NMR spectroscopy: development of a software pipeline. *Proteins* **59**, 687–696.
76. Brunger, A.T., Adams, P.D., Clore, G.M., DeLano, W.L., Gros, P., Grosse-Kunstleve, R.W., et al., (1998). Crystallography & NMR system: a new software suite for macromolecular structure determination. *Acta Crystallogr. D Biol. Crystallogr.* **54**, 905–921.
77. Rieping, W., Habeck, M., Bardiaux, B., Bernard, A., Malliavin, T.E., Nilges, M., (2007). ARIA2: automated NOE assignment and data integration in NMR structure calculation. *Bioinformatics* **23**, 381–382.